Bioorg. Med. Chem. 43 (2021) 116271

Contents lists available at ScienceDirect

Bioorganic & Medicinal Chemistry

journal homepage: www.elsevier.com/locate/bmc

Directed evolution of an amine transaminase for the synthesis of an Apremilast intermediate via kinetic resolution

Chao Xiang [a], Shuke Wu [a,b], Uwe T. Bornscheuer [a,*]

[a] Department of Biotechnology and Enzyme Catalysis, Institute of Biochemistry, University of Greifswald, Felix Hausdorff-Str. 4, 17487 Greifswald, Germany
[b] State Key Laboratory of Agricultural Microbiology, College of Life Science and Technology, Huazhong Agricultural University, No. 1 Shizishan Street, Wuhan 430070, PR China

ARTICLE INFO

Keywords:
Biocatalysis
Chiral amine
Directed evolution
Kinetic resolution
Transaminase

ABSTRACT

Apremilast is an important active pharmaceutical ingredient that relies on a resolution to produce the key chiral amine intermediate. To provide a new catalytic and enzymatic process for Apremilast, we performed the directed evolution of the amine transaminase from *Vibrio fluvialis*. Six rounds of evolution resulted in the VF-8M-E variant with > 400-fold increase specific activity over the wildtype enzyme. A homology model of VF-8M-E was built and a molecular docking study was performed to explain the increase in activity. The purified VF-8M-E was successfully applied to produce the key chiral amine intermediate in enantiopure form and 49% conversion via a kinetic resolution, representing a new enzymatic access towards Apremilast.

1. Introduction

The chiral amine group is a prestigious motif widely found in bioactive natural products and man-made compounds, such as pharmaceuticals and agrochemicals. Many optically pure amines are key chiral building blocks for these bioactive chemicals and are also useful chiral ligands, or chiral reagents for resolution. The common chemical methods to access enantiopure chiral amines include traditional resolution using chiral acids and enantioselective catalysis with metal catalysts and chiral ligands.[1] However, these methods suffer from the use of stoichiometric chiral resolution reagents, or toxic transition metals and costly complex ligands. On the other hand, nature's catalysts, enzymes, provide a catalytic, highly selective, and environmentally friendly alternative method for the production of various chiral chemicals.[2] For the synthesis of chiral amines, the enzyme toolbox includes lipases,[3] transaminases,[4] amine dehydrogenases,[5] monoamine oxidases,[6] and imine reductases.[7] Despite the availability of these enzymes, due to the relatively high substrate specificity, natural enzymes usually require extensive directed evolution[8] for the production of a specific target, especially for the active pharmaceutical ingredients (APIs).[9]

A particularly interesting API containing a chiral amine group is Apremilast, (*S*)-*N*-{2-[1-(3-Ethoxy-4-methoxyphenyl)-2-methanesulfonylethyl]-1,3-dioxo-2,3-dihydro-1*H*-isoindol-4-yl}acetamide.[10] It is an analog of thalidomide and a potent inhibitor of phosphodiesterase 4 and tumor necrosis factor-α.[11] Apremilast was developed by Celgene for the treatment of autoimmune and inflammatory diseases (plaque psoriasis and psoriatic arthritis) under the name of Otezla®. The (*S*)-enantiomer of Apremilast is much more potent than the (*R*)-enantiomer,[10] thus the (*S*)-form was further developed into the API. The original synthetic route to Apremilast involves the resolution of racemic 1-(3-ethoxy-4-methoxyphenyl)-2-(methylsulfonyl)ethanamine (*rac*-**1**) to (*S*)-**1** with stoichiometric *N*-Ac-L-leucine (Scheme 1a).[10] The asymmetric hydrogenation approach had been explored to produce (*S*)-**1** from the corresponding enamine or ketone with precious and toxic rhodium or ruthenium complexes.[12] To our knowledge, there is only one report of an enzyme-mediated synthesis of (*S*)-**1**: lipase (Novozym 435) had been employed for the resolution of *rac*-**1** via acylation,[13] yet the *ee* of acylated product was not perfect.

As part of our research focus on amine transaminases (ATAs),[14–16] we were interested in developing a novel ATA-based method to produce (*S*)-**1** in enantiopure form (Scheme 1b), and thus to provide a catalytic, environmentally friendly, and economic process for Apremilast.

2. Results and discussion

2.1. Identification of a suitable ATA

We screened a range of wild-type (*S*)-selective ATAs and some of

* Corresponding author.
E-mail address: uwe.bornscheuer@uni-greifswald.de (U.T. Bornscheuer).

https://doi.org/10.1016/j.bmc.2021.116271
Received 29 March 2021; Received in revised form 30 May 2021; Accepted 4 June 2021
Available online 10 June 2021
0968-0896/© 2021 Elsevier Ltd. All rights reserved.

their mutants available in our laboratory for the conversion of *rac*-**1** with pyruvate, and analyzed the reaction products by HPLC. Although several wild-type and engineered (*S*)-selective ATAs displayed some activities towards bulky substrates,[14–16] most of them had no detectable activity towards *rac*-**1**. These results indicate the unique structural requirement of **1** in comparison with the bulky amines previously investigated. The only ATA with detectable activity was a double mutant of the ATA from *Vibrio fluvialis* (F85L/V153A, abbreviated as VF-2M), which was previously engineered for (*S*)-phenylbutylamine with a specific activity of 4.99 U/mg.[16a] VF-2M was purified, and its specific activity towards *rac*-**1** was determined by the arylketone assay[17] to be 0.62 mU/mg with pyruvate (Table 1, entry 2). The wildtype VF-ATA had no detectable activity (<0.1 mU/mg), demonstrating the importance of the F85L/V153A mutations for the initial activity.

2.2. Directed evolution of the Vibrio fluvialis ATA

To further improve the activity towards *rac*-**1**, we analyzed the crystal structure of VF-ATA (PDB: 4E3Q)[18] and focused on the residues forming the substrate binding pocket (Figure 1), including 14 residues of the small pocket (F19, L56, F85, F86, R88, R146, W147, V153, K163, Y165, T268, E315, E316), and 11 residues of the large pocket (W57, W150, A228, V258, I259, N286, R415, L417, C424, P426, F427). The residue Y249 at the entry of the substrate binding site was also selected. Using VF-2M as the starting template, single site-saturated mutagenesis of these 26 residues was performed with the Q5 mutagenesis method with NNK codons. For each site, 94 clones were picked and cultured in deep 96-well plates. The activity of VF-ATA variants in the cell lysate was screened for conversion of *rac*-**1** with pyruvate. The characteristic absorbance ($\lambda = 310$ nm) of the corresponding ketone **2**, was measured by a microtiter plate reader.

The iterative saturation mutagenesis (ISM)[19] strategy was applied to improve the activity of VF-ATA. The first round of directed evolution led to the triple mutant VF-3M (bearing an additional W57L mutation) with an activity of 4.38 mU/mg, representing a 7-fold improvement compared to the template VF-2M (Table 1). Using VF-3M as the next template, the second round of directed evolution gave two variants, 4M−A (additional K163A mutation) and 4M−E (additional K163E mutation), with slightly improved activities (Table 1). Further directed evolution pursued two different routes with 4M−A and 4M−E as the templates, respectively (Table 1). The third round of evolution led to 5M−A and 5M−E with the same additional N286C mutation (Table 1). Continuing these two routes gave 6M−A (12.45 mU/mg) and 6M−E (15.40 mU/mg) with the same additional R415K mutation (Table 1). The fifth round of evolution with 6M−A and 6M−E was performed, however, only the 6M−E direction gave a variant, 7M−E (additional F19H mutation), with an improved activity of 32.34 mU/mg (Table 1). The sixth round of evolution of 7M−E led to the best variant, 8M-E (additional Y249F mutation), with an activity of 39.43 mU/mg (Table 1). The VF-8M-E variant thus contains eight mutations: F19H/W57L/F85L/V153A/K163E/Y249F/N286C/R415K. In comparison with the wildtype VF-wt (<0.1 mU/mg) and starting template VF-2M (0.62 mU/mg), the final VF-8M-E variant displays > 400-fold and > 60-fold increased activity, respectively.

Table 1
VF-ATA variants and their corresponding activity towards *rac*-**1**/pyruvate, *rac*-**1**/pentanal[a].

Variant	Mutation	Specific Activity [mU/mg]	
		Pyruvate	Pentanal
VF-wt	–	< 0.1	< 0.1
2M	**F85L/V153A**	0.62 ± 0.07	0.49 ± 0.34
3M	**W57L**/F85L/ V153A	4.38 ± 0.12	0.96 ± 0.09
4M−A	W57L/F85L/V153A/**K163A**	5.43 ± 0.03	2.26 ± 0.11
4M−E	W57L/F85L/V153A/**K163E**	6.01 ± 0.07	4.42 ± 0.12
5M−A	W57L/F85L/V153A/K163A/**N286C**	8.06 ± 1.41	4.20 ± 0.33
5M−E	W57L/F85L/V153A/K163E/**N286C**	8.65 ± 0.23	6.03 ± 0.33
6M−A	W57L/F85L/V153A/K163A/N286C/**R415K**	12.45 ± 0.16	13.38 ± 0.23
6M−E	W57L/F85L/V153A/K163E/N286C/**R415K**	15.40 ± 0.55	20.95 ± 0.36
7M−E	**F19H**/W57L/F85L/V153A/K163E/N286C/R415K	32.34 ± 1.82	14.86 ± 0.48
8M-E	F19H/W57L/F85L/V153A/K163E/**Y249F**/N286C/R415K	39.43 ± 3.68	n.m.[b]

[a] Arylketone assay conditions: The specific activities of the purified VF-ATA variants for the conversion of *rac*-**1** were determined by using the arylketone assay in 96-well microtiter plates, and measured on the Infinite® 200 PRO (TECAN) plate reader. The assay was performed with *rac*-**1** (5 mM) as amine donor and pyruvate (2.5 mM) or pentanal (2.5 mM) as amine acceptors in DMSO (1.25–2.5%), HEPES buffer (50 mM, pH 6.5) at 30 °C. The formation of **2** was quantified by following the increase of absorption at 310 nm over time. One unit (U) was defined as the formation of 1 μmol **2** per minute. All measurements were performed in triplicates.
[b] n.m. = not measured.

2.3. Characterization of the best three variants of VF-ATA

The best three variants, VF-6M−E, VF-7M−E, and VF-8M-E, were selected for further characterization. Because the protein engineering rounds were performed with *rac*-**1**, we further examined the enantioselectivity of the three variants for converting (*S*)-**1**. Fortunately, all the VF-ATA variants did not show any detectable activity towards (*S*)-**1** (<0.1 mU/mg). This proved the excellent enantioselectivity of VF-ATA

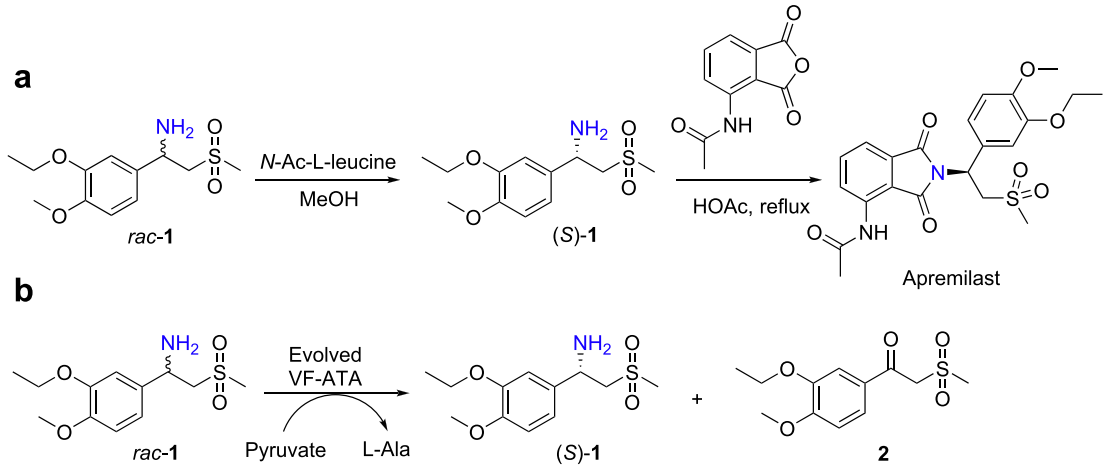

Scheme 1. **a** The original synthetic route to Apremilast involves resolution of *rac*-**1** to (*S*)-**1**. **b** Kinetic resolution of *rac*-**1** to (*S*)-**1** by the evolved VF-ATA.

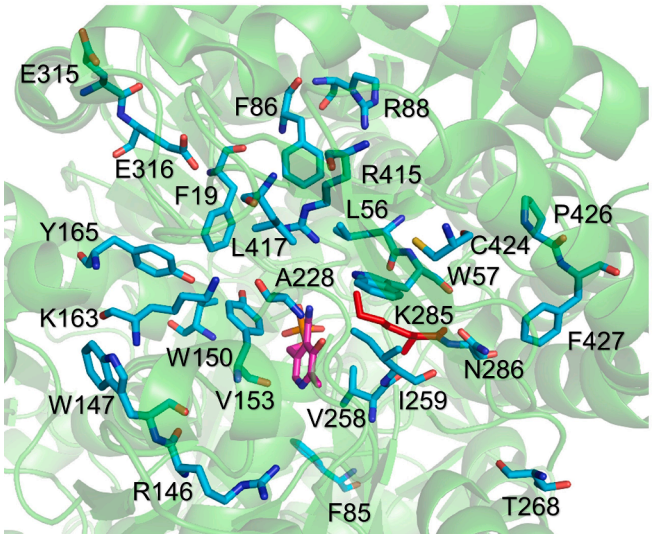

Figure 1. Structure of VF-ATA (PDB: 4E3Q) with the key residues labeled. Key residues are shown as sticks: pyridoxamine-5′-phosphate (PMP) in pink, the catalytic lysine (K285) is highlighted in red, other sites for mutation are in blue.

variants. The three variants were purified and tested in different reaction buffer (Figure 2). The maximum specific activity was achieved at the optimal pH of 6.0 or 6.5. Then, the best three variants were applied for the kinetic resolution of *rac*-**1** under the optimal conditions. As shown in Figure 3, 20 mM of *rac*-**1** was resolved by VF-8M-E in 24 h to reach 51% conversion, while VF-7M−E and VF-6M−E took 48 h to reach > 50% conversion. The optical purity of the remaining (*S*)-**1** at 48 h was determined to be > 99% *ee*. During the reaction, a small percentage (~10%) of byproduct 1-(3-ethoxy-4-methoxyphenyl)ethenone was observed, probably due to the α,β-elimination of (*R*)-**1**. Nevertheless, these results demonstrated that the highly enantioselective VF-ATA variants could be applied to produce the enantiopure amine intermediate for Apremilast. The unpurified cell lysates were also proven as catalysts for the kinetic resolution (see Figure S2 in SI). To demonstrate the synthetic application, the kinetic resolution was performed on 20 mL scale (100 mg) using the stable variant (VF-6M−E). The reaction took 48 h to reach a conversion of 50%. Simple workup (filtration, extraction, and evaporation) afforded (*S*)-**1** (>99% *ee*) in 41% isolated yield, and ketone **2** in 43% isolated yield.

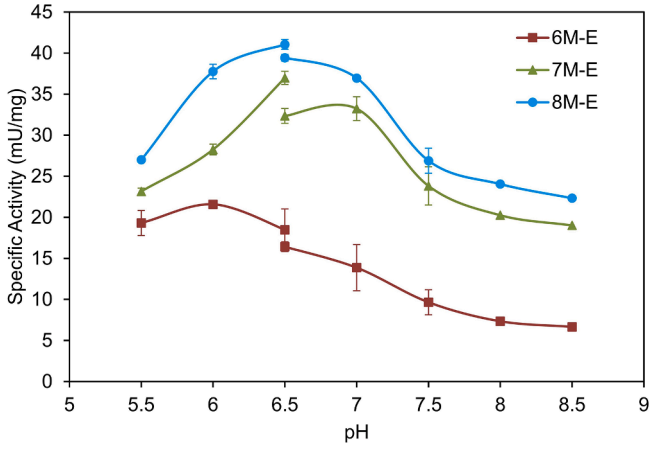

Figure 2. Specific activity of the best three VF-ATA variants for conversion of *rac*-**1** in different buffers. Assay conditions: 5 mM *rac*-**1**, 50 mM potassium phosphate buffer (pH 5.5–6.5) or HEPES buffer (pH 6.5–8.5), 0.1 mM PLP, 2.5 mM pyruvate, 1% (vol/vol) DMSO, 30 °C.

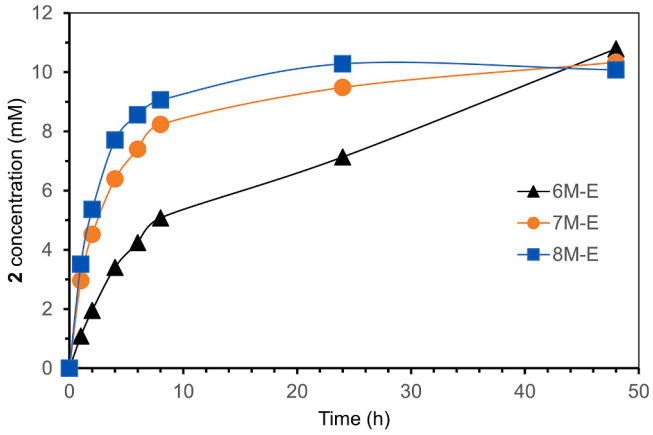

Figure 3. Kinetic resolution of *rac*-**1** with the best three VF-ATA variants. Assay conditions: 20 mM *rac*-**1**, 50 mM HEPES buffer pH 6.5, 0.1 mM PLP, 200 mM pyruvate, 10% (vol/vol) DMSO, 0.3–0.8 mg/ml purified enzyme, 37 °C and 180 rpm.

2.4. Homology modeling and docking study of VF-8M-E

To elucidate the possible mechanism and the molecular rational for the observed improved activity towards *rac*-**1**, a homology model of the VF-8M-E was built with YASARA. As shown in Figure 4a and 4b, in comparison to the wildtype VF-wt, the substrate binding pocket was significantly expanded in the VF-8M-E variant, which hence can now accommodate the bulky substrate (*R*)-**1** much better. The molecular docking of the reaction intermediate, PLP-(*R*)-**1** complex, to the model of VF-8M-E was simulated with YASARA. As depicted in Figure 4c, the position of PLP in VF-8M-E was very similar to that of PMP in VF-wt, which validated that PLP-(*R*)-**1** complex was docked in a reasonable conformation. It is clear that, the W57L and R415K mutations significantly expanded the substrate binding pocket to accommodate the challenging methylsulfonyl group. On the other side of the binding pocket, F19H, F85L, and V153A contributed to host the 3-ethoxy-4-methoxyphenyl group. The contribution of the other three mutations is minor.

3. Conclusion

To provide a new enzymatic access to the chiral amine intermediate (*S*)-**1** for the synthesis of Apremilast, we identified a double mutant of the ATA from *Vibrio fluvialis*, which had initial activity for the conversion of *rac*-**1**. Subsequently, six rounds of directed evolution resulted in the VF-8M-E variant with > 60-fold increase specific activity. A homology model of VF-8M-E was built and molecular docking study was performed to explain the increase of activity. The purified VF-8M-E was successfully applied in the kinetic resolution of *rac*-**1** to produce enantiopure (*S*)-**1** in 49% conversion. The preparative kinetic resolution was performed with the stable variant VF-6M−E to afford enantiopure (*S*)-**1** in 41% isolated yield. The application of this ATA variant represents an alternative method for the synthesis of the key chiral amine intermediate for the manufacturing of Apremilast.

4. Experimental section

4.1. Site-directed mutagenesis

All variants were prepared using Q5® site-directed mutagenesis kit from New England BioLabs. The degenerated primers were designed non-overlapping by using the standard setting of NEBaseChanger. For the PCR, template plasmid (0.25 ng/μL, carrying the VF-2M gene), forward and reverse primers (0.5 μM each), Q5® hot start high-fidelity

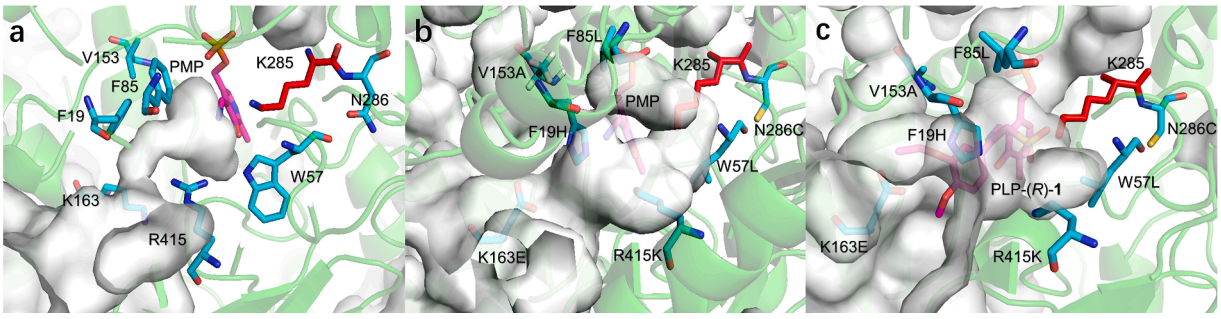

Figure 4. Structural study of VF-wt and VF-8M-E. **a** The substrate binding pocket of VF-wt; **b** the substrate binding pocket of the homology model of VF-8M-E; **c** docking of PLP-(*R*)-**1** complex to the model of VF-8M-E. The PMP and PLP-(*R*)-**1** are in pink, the catalytic lysine (K285) is highlighted in red, and the mutated residues are highlighted in blue.

2X master mix were used. The PCR was performed as follows: (i) 98 °C, 30 s; (ii) 30 cycles: 98 °C, 10 s; 50–72 °C, 30 s; 72 °C, 0.5 min/kbp; (iii) 72 °C, 2 min. The resulting PCR product was directly treated with the kinase, ligase & *Dpn*I (KLD enzyme mix; NEB) at room temperature for 30 min and then transformed in chemically competent *E. coli* TOP10 cells. After confirmation of the codon distribution in the case of site-saturation mutagenesis, the PCR products were transformed in chemical competent *E. coli* BL21(DE3) cells for expression.

4.2. Protein expression and purification of the enzyme variants

The plasmid constructs containing the genes of VF-ATA variants were transformed into *E. coli* BL21(DE3) cells, and the resulted cells were incubated in an LB-medium (Lysogeny Broth, 5 mL) preculture with kanamycin (50 μg/mL) at 37 °C overnight. The preculture was transferred into TB-medium (Terrific Broth, 100 mL) with kanamycin (50 μg/mL) and incubated at 37 °C, 180 rpm. The expression of the Vf-ATA variants was induced with IPTG (0.5 mM, isopropyl β-D-thio-galactopyranoside) at an optical density of approx. 0.6 at 600 nm, and incubated at 26 °C overnight. The cells were harvested by centrifugation (20 min, 4000 g).

For purification of the VF-ATA variants, the cell pellets were resuspended in HEPES buffer (50 mM, pH 7.5) containing NaCl (300 mM), PLP (0.1 mM), imidazole (10 mM), and then lysed by ultrasonication (50% power, 50% pulse, 2 × 5 min). The lysate was clarified by centrifugation (1 h, 10,000 g, 4 °C) and purified by affinity chromatography (Ni-NTA agarose) with the following buffers: washing buffer containing HEPES (50 mM, pH 7.5) PLP (0.1 mM), NaCl (300 mM), and imidazole (20 mM), and elution buffer containing HEPES (50 mM, pH 7.5) PLP (0.1 mM), NaCl (300 mM), and imidazole (300 mM). The VF-ATAs were desalted in HEPES buffer (50 mM pH 7.5) with PLP (0.1 mM) using the PD-10 desalting column (GE Healthcare). The purified VF-ATAs were stored in 30% glycerol at −20 °C.

4.3. Determination of activity of VF-ATA variants

The specific activities of the purified VF-ATA variants for the conversion of *rac*-**1** were determined by using the arylketone assay in 96-well microtiter plates, and measured on the Infinite® 200 PRO (TECAN) plate reader. The assay was performed with *rac*-**1** (5 mM) as amine donor and pyruvate (2.5 mM) or pentanal (2.5 mM) as amine acceptors in DMSO (1.25–2.5%), HEPES buffer (50 mM, pH 6.5) at 30 °C. The formation of **2** was quantified by following the increase of absorption at 310 nm over time.

4.4. Kinetic resolution of rac-1 with VF-ATA variants

To a 100-mL flask, the following components were added to form a 10-mL system: HEPES buffer (50 mM, pH 6.5) with PLP (0.1 mM), *rac*-**1** (20 mM), pyruvate (200 mM), DMSO (10%), purified VF-ATA (0.3–0.8 mg/mL). The reaction was incubated in a shaking incubator at 37 °C and 180 rpm. At 1, 2, 4, 6, 8, 24, and 48 h of the reaction, samples (100 μL) were taken and mixed with acetonitrile (500 μL) and trifluoracetic acid solution (0.1%, 400 μL) for HPLC analysis of the conversion of **1**. The samples (125 μL) were basified with NaOH (100 mM, 125 μL) and extracted with ethyl acetate (0.5 mL). The organic phase was dried over Na_2SO_4, filtered and the supernatant was subjected to evaporation. The dried residues were diluted in a mixture of hexane/ethanol/isopropanol (50:40:10) for chiral HPLC analysis of *ee*.

4.5. Preparation of (S)-1 with VF-ATA variants

To a 100-mL flask, HEPES buffer (50 mM, pH 6.5, including 0.1 mM PLP and 100 mM pyruvate), *rac*-**1** (100 mg), and purified VF-6 M−E (20 mg) were added to form a 20 mL reaction volume system. The reaction was maintained at pH 6.5 and 30 °C until reaching 50% conversion analyzed by HPLC. Afterwards, the reaction was quenched with HCl (100 mM) to pH 2.0 and the mixture was filtered. The filtrate was washed with CH_2Cl_2 (2 × 5 mL) and then NaOH solution (1 M) was added to adjust the pH to 12. The basified solution was extracted with CH_2Cl_2 (2 × 25 mL), and the CH_2Cl_2 was evaporated to afford (*S*)-**1** (41 mg, 41% yield) as yellow solid. ^{1}H NMR (DMSO-d_6) δ: 7.02 (m, 1H), 6.89 (m, 2H), 4.28–4.23 (m, 1H), 4.03–3.98 (q, J = 6.9 Hz, 2H), 3.73 (s, 3H), 3.45–3.20 (m, 2H), 2.96 (s, 3H), 2.07 (brs, 2H), 1.35–1.30 (t, J = 6.9 Hz, 3H). To isolate **2**, the solid of the initial filtration was washed with HCl (100 mM), dissolved in acetonitrile, and filtered again, the filtrate was evaporated to give ketone **2** (43 mg, 43% yield) as white solid. ^{1}H NMR (DMSO-d_6) δ: 7.73–7.72 (m, 1H), 7.50–7.49 (m, 1H), 7.13–7.09 (m, 1H), 5.04 (s, 2H), 4.13–4.05 (q, J = 7.2 Hz, 2H), 3.87 (s, 3H), 3.13 (s, 3H), 1.38–1.32 (t, J = 7.2 Hz, 3H).

Declaration of Competing Interest

The authors declare that they have no known competing financial interests or personal relationships that could have appeared to influence the work reported in this paper.

Acknowledgments

X. C. thanks the China Scholarship Council for financial support of a PhD thesis project (File No.: 201808330394). S. W. thanks the Alexander von Humboldt-Stiftung for a Humboldt Research Fellowship. The authors thank Ina Menyes for support with HPLC analysis.

Appendix A. Supplementary material

Supplementary data to this article can be found online at https://doi.org/10.1016/j.bmc.2021.116271.

References

1 (a) Breuer M, Ditrich K, Habicher T, et al. *Angew Chem Int Ed.* 2004;43:788–824. https://doi.org/10.1002/anie.200300599;
(b) Nugent TC, El-Shazly M. *Adv Synth Catal.* 2010;352:753–819. https://doi.org/10.1002/adsc.200900719.

2 (a) Sheldon RA, Brady D, Bode ML. *Chem Sci.* 2020;11:2587–2605. https://doi.org/10.1039/C9SC05746C;
(b) Hauer B. *ACS Catal.* 2020;10:8418–8427. https://doi.org/10.1021/acscatal.0c01708;
(c) Hollmann F, Opperman DJ, Paul CE. *Angew Chem Int Ed.* 2021;60:5644–5665. https://doi.org/10.1002/anie.202001876;
(d) Winkler CK, Schrittwieser JH, Kroutil W. *ACS Cent Sci.* 2021;7:55–71. https://doi.org/10.1021/acscentsci.0c01496;
(e) Wu S, Snajdrova R, Moore JC, Baldenius K, Bornscheuer UT. *Angew Chem Int Ed.* 2021;60:88–119. https://doi.org/10.1002/anie.202006648;
(f) Marshall JR, Mangas-Sanchez J, Turner NJ. *Tetrahedron.* 2021;82. https://doi.org/10.1016/j.tet.2021.131926.

3 (a) Ghislieri D, Turner NJ. *Top Catal.* 2014;57:284–300. https://doi.org/10.1007/s11244-013-0184-1;
(b) Kohls H, Steffen-Munsberg F, Höhne M. *Curr Opin Chem Biol.* 2014;19:180–192. https://doi.org/10.1016/j.cbpa.2014.02.021.

4 (a) Hohne M, Bornscheuer UT. *ChemCatChem.* 2009;1:42–51. https://doi.org/10.1002/cctc.200900110;
(b) Koszelewski D, Tauber K, Faber K, Kroutil W. *Trends Biotechnol.* 2010;28:324–332. https://doi.org/10.1016/j.tibtech.2010.03.003;
(c) Tufvesson P, Lima-Ramos L, Jensen JS, Al-Haque N, Neto W, Woodley JM. *Biotechnol Bioeng.* 2011;108:1479–1493. https://doi.org/10.1002/bit.23154;
(d) Mathew S, Yun H. *ACS Catal.* 2012;2:993–1001. https://doi.org/10.1021/cs300116n;
(e) Fuchs M, Farnberger JE, Eur KW. *J Org Chem.* 2015;6965–6982. https://doi.org/10.1002/ejoc.201500852;
(f) Steffen-Munsberg F, Vickers C, Kohls H, et al. *Biotechnol Adv.* 2015;33:566–604. https://doi.org/10.1016/j.biotechadv.2014.12.012;
(g) Guo F, Berglund P. *Green Chem.* 2017;19:333–360. https://doi.org/10.1039/C6GC02328B;
(h) Slabu I, Galman JL, Lloyd RC, Turner NJ. *ACS Catal.* 2017;7:8263–8284. https://doi.org/10.1021/acscatal.7b02686;
(i) Kelly SA, Pohle S, Wharry S, et al. *Chem Rev.* 2018;118:349–367. https://doi.org/10.1021/acs.chemrev.7b00437;
(j) Gomm A, O'Reilly E. *Curr Opin Chem Biol.* 2018;43:106–112. https://doi.org/10.1016/j.cbpa.2017.12.007;
(k) Patil MD, Grogan G, Bommarius A, Yun H. *Catalysts.* 2018;8:254. https://doi.org/10.3390/catal8070254;
(l) Rocha JF, Pina AF, Sousa SF, Cerqueira NMFSA. *Catal Sci Technol.* 2019;9:4864–4876. https://doi.org/10.1039/C9CY01210A.

5 Grogan G. *Curr. Opin. Chem. Biol.* 2018;43:15–22.

6 Batista VF, Galman JL, Pinto DCGA, Silva AMS, Turner NJ. *ACS Catal.* 2018;8:11889–11907.

7 Mangas-Sanchez J, Montgomery SL, Aleku GA, et al. *Curr. Opin. Chem. Biol.* 2017;37:19–25.

8 (a) Zeymer C, Hilvert D. *Ann Rev Biochem.* 2018;87:131–157. https://doi.org/10.1146/annurev-biochem-062917-012034;
(b) Angew AFH. *Chem Int Ed.* 2019;58:14420–14426. https://doi.org/10.1002/anie.201907729;
(c) Bornscheuer UT, Hauer B, Jaeger KE, Schwaneberg U. *Angew Chem Int Ed.* 2019;58:36–40. https://doi.org/10.1002/anie.201812717;
(d) Qu G, Li A, Acevedo-Rocha CG, Sun Z, Reetz MT. *Angew Chem Int Ed.* 2020;59:13204–13231. https://doi.org/10.1002/anie.201901491.

9 (a) Patel RN. *Bioorg Med Chem.* 2018;26:1252–1274. https://doi.org/10.1016/j.bmc.2017.05.023;
(b) Sun H, Zhang H, Ang EL, Zhao H. *Bioorg. Med. Chem.* 2018;26:1275–1284. https://doi.org/10.1016/j.bmc.2017.06.043;
(c) Li G, Wang J, Reetz MT. *Bioorg. Med. Chem.* 2018;26:1241–1251. https://doi.org/10.1016/j.bmc.2017.05.021;
(d) Adams JP, Brown MJB, Diaz-Rodriguez A, Lloyd RC, Roiban G. *Adv. Synth. Catal.* 2019;361:2421–2432. https://doi.org/10.1002/adsc.201900424;
(e) Albarrán-Velo J, González-Martínez D, Gotor-Fernández V. *Biocatal. Biotransformat.*. 2018;36:102–130. https://doi.org/10.1080/10242422.2017.1340457;
(f) Fryszkowska A, Devine PN. *Curr. Opin. Chem. Biol.* 2020;55:151–160. https://doi.org/10.1016/j.cbpa.2020.01.012.

10 Man H-W, Schafer P, Wong LM, et al. *J. Med. Chem.* 2009;52:1522–1524.

11 (a) Schett G, Sloan VS, Stevens RM, Schafer P. *Ther. Adv. Musculoskel. Dis.* 2010;2:271–278. https://doi.org/10.1177/1759720X10381432;
(b) Papp K, Reich K, Leonardi CL, et al. *J. Am. Acad. Dermatol.* 2015;73:37–49. https://doi.org/10.1016/j.jaad.2015.03.049.

12 Ruchelman AL, Connolly TJ. *Tetrahedron Asymmetry*. 2015;26:553–559.

13 Doubsky, J.; Klvana, R.; Richter, J.; Lehnert, P. WO2016192694, 2016.

14 Pavlidis IV, Weiß MS, Genz M, et al. *Nat. Chem.* 2016;8:1076–1082.

15 Voss M, Das D, Genz M, et al. *ACS Catal.* 2018;8:11524–11533.

16 (a) Nobili A, Steffen-Munsberg F, Kohls H, et al. *ChemCatChem.* 2015;7:757–760. https://doi.org/10.1002/cctc.201403010;
(b) Genz M, Vickers C, van denBergh T, et al. *Int. J. Mol. Sci.* 2015;16:26953–26963. https://doi.org/10.3390/ijms161126007;
(c) Genz M, Melse O, Schmidt S, et al. *ChemCatChem.* 2016;8:3199–3202. https://doi.org/10.1002/cctc.201601007.

17 Schätzle S, Höhne M, Redestad E, Robins K, Bornscheuer UT. *Anal. Chem.* 2009;81:8244–8248.

18 Midelfort KS, Kumar R, Han S, et al. *Protein Eng. Des. Sel.* 2013;26:25–33.

19 Reetz MT, Carballeira JD. *Nat. Prot.* 2007;2:891–903.